Experimental and Numerical Simulation of an Airlift Pump with Conventional and Modified Air Injection Device

Ali Abdul Mohsin Hasan Alasadi
Assistant Professor
College of Engineering-University of Baghdad
dralicit @yahoo.com

Ahmed Khalid Habeeb
M.Sc.
College of Engineering-University of Baghdad
eng_ahmedkhalid@yahoo.com

ABSTRACT

The effect of air injection device on the performance of airlift pump used for water pumping has been studied numerically and experimentally. An airlift pump of dimensions 42mm diameter and 2200 mm length with conventional and modified air injection device was considered. A modification on conventional injection device (normal air-jacket type) was carried out by changing injection angle from 90° (for conventional) to 22.5° (for modified). Continuity and Navier-Stokes equations in turbulent regime with an appropriate two-phase flow model (VOF) and turbulent model ($k-\epsilon$) in two dimensions axisymmetry flow were formulated and solved by using the known package FLUENT version (14.5). The numerical and experimental investigations were carried out for both conventional and unconventional air-jackets at submergence ratio of 0.75 and air mass flow rate from 0.5, 2, 10, 50 and 85 kg/hr. Comparisons between the numerical and experimental results for both injection devices were made and fair agreements were found and the main results showed that the performance and maximum efficiency of airlift pump is increased for higher mass flow rate of injected air for the tested submergence ratio using unconventional air-jacket performance with average enhancement were 9% and 10% for performance and maximum efficiency respectively.

Key words: airlift pump, air injection angle, submergence ratio, two-phase flow

تمثيل عددي لمضخة رفع هوائية باستخدام جهاز حقن تقليدي وجهاز أخر معدل

علي عبد المحسن حسن الاسدي
أستاذ مساعد
كلية الهندسة-جامعة بغداد

احمد خالد حبيب
ماجستير
كلية الهندسة-جامعة بغداد

الخلاصة

تم إجراء دراسة تحليلية وعملية حول تأثير زاوية حقن الهواء على أداء مضخات الرفع الهوائية التي تستخدم في رفع الماء. تم الأخذ بنظر الاعتبار مضخة رفع هوائية بقطر 42 ملم لأنبوب الرفع وبطول 2200 ملم باستخدام منظومة حقن هواء تقليدية ومنظومة أخرى معدلة. تم تعديل منظومة حقن الهواء التقليدية نوع (Air-Jacket) من خلال تغير زاوية الحقن من 90 درجة (للمنظومة التقليدية) إلى زاوية 22.5 درجة (للمنظومة المعدلة). اعتمدت الدراسة العددية على قانون حفظ الكتلة وقانون الزخم لنافير ستوك ضمن منطقة الجريان الاضطرابي مع موديل (VOF) الخاص بالجريان ثنائي الأطوار باستخدام موديل ($k-\epsilon$) ثنائي الإبعاد متناظر حول المركز. هذا الموديل تم نمذجته باستخدام برنامج الفلونت إصدار14.5. وتم إجراء الحل الرياضي والفحص العملي للمضخة مع منظومة حقن تقليدية ومعدلة عند نسبة غمر مقدارها 0.75 مع معدل تدفق كتلة الهواء المحقون من 0.5، 2، 10، 50، 85 كغم/ساعة والتي تغطي كل أنماط الجريان المحتمل حدوثها داخل الأنبوب الصاعد. بينت المقارنة بين النتائج التحليلية والنتائج العملية مقبولية عالية وقد أظهرت النتائج زيادة في أداء وكفاءة المضخة عند معدلات الحقن العالية عند استخدام منظومة الحقن المعدلة لكل ظروف الفحص مع تحسن 9% في الأداء و 10% لأعلى كفاءة.

الكلمات الرئيسية: مضخات الرفع الهوائية، زاوية حقن للهواء، نسبة الغمر، جريان ثنائي الطور

1. INTRODUCTION

The first airlift pump was discovered by the German mining engineer Garl E. Loescher in 1797 and it used for the first time in United States in 1846 in oil field in Pennsylvania. Although, submersible rotodynamic pumps have been used successfully for the first time in 1928 in oil field and become widely used in many other applications, airlift pump are still utilized in several specialized tasks, **Aaron, 2004**. Airlift pump has a number of advantages that promoted to use it, such as: low initial cost, no moving parts when compared with other types, easy installation and small space requirement, simplest design and construction, low cost for maintenance, ability to resist clogging, ease of flow controlling and the ability of handle corrosive, explosive, highly toxic and radioactive fluids. It is classified as deep well pumps and sometimes used for dewatering of mines or pumping mixture of sand and water slurry or other solution. In the last several decades, the development of the digital computer has enabled to make an accurate design of airlift pump by solving more complex methods that include solving the Navier-Stokes equations with governing equation of multi-phase flow at various points in the airlift pump to determine the nature of the flow. The flow solver procedure, frequently mentioned to as Computational Fluid Dynamics (CFD) are less restricting but large computationally intense to solve. **Li et al., 2012,** evaluated the performance of small airlift pump with diameter range of 12-19 mm and length of 0.933 m at various submergence ratios using FLUENT. The domain of the simulation is represented by two dimensional axisymmetry systems, and volume of fluid (VOF) model is used to perform the simulation with a time step of 0.001 s. They predicted that more accurate simulation is associated with submergence ratio under 0.5 when the results are compared with the experimental result available in the literature, as well as more fluctuation and more instability of velocity with the vertical uprising position when higher mass flow rate is introduced to the riser. **Wahba et al., 2014,** investigated a hierarchy of models that is used for obtaining the performance of airlift pumps, from one-dimensional analytical models of**, Stenning and Martin, 1968,** and, **Reinemann et al., 1986,** to large eddy simulation (LES) using the volume of fluid (VOF) method and the results of investigated models are validated with experimental results of, **Kassab et al., 2009**. They reported that LES method gives fairly accurate results for the performance of airlift pump with a good qualitative and quantitative flow patterns when compared with their similar experimental patterns at the same air flow rate, and with flow pattern map proposed by, **Taitel et al., 1980**. Also they reported that the analytical models provide pump performance curve with accuracy comparable to that predicted by LES; but without any knowledge about flow patterns in the riser pipe and the transient nature of the pumping process due to the steady state nature of these models. **Hanafizadeh et al., 2014,** modeled numerically the two phase flow regimes in the riser of airlift pump using two different approach of modeling, namely volume of fluid (VOF) and Eulerian, with standard k-Ɛ turbulent model and cylindrical coordinates to represent the geometry. The results are validated with the flow regime map proposed by, **Taitel et al., 1980,** as well as with experimental results. The experimental work is carried out using three different configuration of injector plate. They reported that the VOF model is fit better for modeling of bubbly and slug flows while the Eulerain model is more suitable for only annular flow. **Mahrous, 2014,** studied numerically the effects of multistage air injection on the performance of airlift pump when the compressed air is evenly distributed in a number of injection stages in the riser tube section. He performed the numerical solution by dividing the riser pipe into small division in the flow direction and step-by-step integration method to the momentum balance equation along the riser pipe to obtain the performance. He showed that expanding of bubbly-slug flow regime rang in the riser tube of airlift pump is corresponded to

increasing in number of injection stages which is result widening in operation range of the pump close to the optimum discharge conditions, and at these operation conditions, the stability of airlift pump using multi-stage air injection is increased when compared with single-stage air injection. **Qingsong Zhan et al., 2015,** investigated numerically the effect of the riser pipe diameter and length on the efficiency of airlift pump used in artificial upwelling process for ocean water. Numerically, the CFD model employed finite difference method (FEM) to discretize the flow which is represented in two-dimensional coordinates system, transient solver, VOF model and standard k-Ɛ turbulent model to solve the problem. The time interval set to 0.0001 s to increase the convergence of the solution. They indicated that the pipe diameter is more effective than the pipe length, increasing of riser diameter led to increase of lifting efficiency, also, increasing of pipe length causes slightly decreasing in the efficiency because of wall friction increased in stable flow field.

In the present work, the performance of a regular airlift pump with conventional air-jacket and modified air-jacket are investigated numerically and experimentally at fixed submergence ratios and various mass flow rate of injected air.

2. EXPERIMENTAL WORK

The experimental work has been carried out in the fluid mechanics laboratory in the department of mechanical engineering - Collage of engineering/University of Baghdad in order to obtain water discharge rate and analysis the structure of flow filed within riser pipe. The experimental setup is shown in **Fig.1 and Fig.2.**

2.1 Test Rig

The test rig consists of the riser pipe which is a transparence smooth pipe made of acrylic resin with 2000 mm length and 42mm inner diameter. The discharge side (upper end) of the riser pipe is connected to a collecting header of 4" diameter made of PVC. The highest point of the header is opened to ambient which allows air to escape from the pumped mixture. The lower end of the collecting header is divided in to two branches with 2" PVC quick closing ball valve at its end to direct water from riser either, to intermediate tank or to metering tank. A 0.5 hp electric centrifugal water pump has maximum head of 35 m and maximum discharge of 36 litters/minute, is used to pump water from the intermediate tank to the movable tank. The movable tank is a cylindrical tank hold by steel cable connected to a manual hoist and can be moved upward and downward in order to change the submergence ratio and feed the riser pipe with water at constant head through the transient tank. A 1" ball valve is fitted at the bottom side of the transient tank as inlet to the tank. The riser pipe is fitted to the transient tank through the injection device, in which the compressed air is distributed uniformly and injected into the riser pipe to perform the pumping action. The injection device is designed as two independent injection stages. Each stage delivered air through two ports and have 52 holes per stage drilled of diameter 3mm distributed in two rows and holes center line are inclined from injector wall by 90° and 22.5° for the first and second stages respectively. Injection device with holes center line vertical to the injector wall (90°) is considered as normal or standard air jacket. **Fig.3** shows the cross section of injection device. All the elements above of the test rig are assembled to gather in a main steel frame. The experimental work is performed using a high pressure air compressor which delivered 1.05 m^3/min with a storage vessel of 1200 lit capacity and cutoff pressure sited to 14 bar, this compressor supply compressed air to a pressure reducing valve (0.5 – 5) bar to ensure a constant air pressure supply from the compressor. A constant area air flow meter of range (2 – 27) m^3/hr is used to measure the volume flow rate of injected air and the

temperature of supplied air was measured by a calibrated thermocouple. A needle valve 3/4" is used to control the volume flow rate of injected air to the rig, as well as a 3/4" ball valve made is used to simultaneously cutoff air supplying to the rig.

2.2 Experimental Procedure

The main part of the experiment was the measuring of the water discharged from the airlift pump for different angles of injection. The experimental procedures are as follows:

1. The air compressor is started; the pressure reducing valve is adjusted to the desired pressure.
2. The connection hose of the air system is linked to the desired stage of injection.
3. The centrifugal pump is started.
4. The level of movable tank is adjusted to the desired submergence ratio.
5. Injection of compressed air into the pipe is started, the needle valve is adjusted to desired volume flow rate(Q_{air}), and then the pressures(P_{air}) and temperature(T_{air}) are recorded.
6. The air mass flow rate is computed from the following equation:

$$\dot{m}_{air} = \rho_{air} \times Q_{air} \quad (1)$$

Where the density of air is calculated using ideal gas equation:

$$\rho_{air} = \frac{P_{air}}{R \times T_{air}} \quad (2)$$

7. Waiting until the system reach quasi- steady state.
8. The discharged water from intermediate tank is directed to the metering tank for a certain time (usually is taken 20 s) by closing the valve at the end of the collecting header which is routed the water to the intermediate tank and open the other to the metering tank:
9. The volume of water accumulated in the metering tank ($V_{accumilate}$) is recorded.
10. The water mass flow rate is computed from the following equation

$$\dot{m}_{water} = \rho_{water} \times \frac{V_{accumilate}}{t} \quad (3)$$

11. An estimation of flow regime type is reported.
12. Simultaneously closing the ball valves 14 and 15, **Hamid et al., 2013**:
13. The retained volume of the riser (V_L) is recorded and the volumetric void fraction is computed from the equation:

$$\alpha = 1 - \frac{V_L}{total\ volume\ of\ riser} \quad (4)$$

(7) and (8) are repeated three times for each mass flow rate of air and the average results are taken.

The procedure above is repeated for different submergence ratio and injection angle for the same range of air mass flow rate.

A high speed camera made by SAMSUNG (model WB2000, 10 megapixels and 1000 f/s) is used to capture photos of flow regime detected in the riser tube, and water is colored by adding a light color in order to make the reorganization of flow pattern easier.

2.3 Error Analysis

Deviation was calculated for the experimental data using the formula for calculating percentage error as:

$$Percentage\ error\ = \left(\frac{measured\ value - estimated\ value}{measured\ value}\right) * 100 \quad (5)$$

Where measured values are resulted from the experimental work and the estimated value from the theoretical.

3. MATHMATICAL FORMULATION

In computational fluid dynamics, the volume of fluid model is one of Euler – Euler method which is used in numerical modeling of multiphase flow and it is considered the model that enables clear description of fluids interface by tracking and locating the fluids interface, **Hirt and Nichols, 1982,** and, **Li et al., 2012**. The concept of the model is based on treating the different phases of fluids as interpenetrated continua and volume of a phase cannot occupy by other phases. In talking on multiphase flow and specifically two-phases flow of water and air in airlift pump, water is considered the primary or continues phase that is enveloping the secondary phase (air) which is distributed in the primary phase in flow field therefore, a place in flow field may be filled by only water or only air or both water-air in interfaces, and the flow of water-air interface is tracked depending on the distribution of the volume fraction of air in flow field. Numerical techniques have to be employed to solve Navier-Stokes, continuity and volume fraction equations by using the Finite Volume Method.

3.1 Governing Partial Differential Equations

In the present work, the working fluids are water and air and the following assumptions are made:

1- Axisymmetric flow.
2- Fully turbulent flow.
3- Newtonian fluid.
4- No exchange of mass between phases.
5- No heat transfer and heat generation.
6- Isothermal flow for all phases.
7- Incompressible for the air phase.

In order to analyze the flow field and the performance in the airlift pump with variable geometrical and operation parameters, VOF model solves one set of momentum equations for the whole flow and tracking the volume fraction of each phase of the mixture through the flow field. The governing equations for the mean velocity and pressure are the mass and momentum equations, these are respectively**, Fluent, 2012,** and**, Li et, al., 2012**:

$$\frac{\partial}{\partial t}(\rho\,\vec{u}) + \nabla.(\rho\,\vec{u}\,) = 0 \tag{6}$$

$$\frac{\partial}{\partial t}(\rho\,\vec{u}) + \nabla.(\rho\,\vec{u}\,\vec{u}\,) = \rho\vec{g} - \nabla P + \nabla.[\mu(\nabla\,\vec{u} + \nabla\,\vec{u}^{\,T})] + \overrightarrow{T} \tag{7}$$

The tracking of volume fraction of gas phase for air and water flow neglecting the mass transfer between phases is performed by solving the convection equation for volume fraction as following, **Fluent, 2012,** and**, Li et al., 2012**:

$$\frac{1}{\rho_g}\left[\frac{\partial}{\partial t}\left(\alpha_g\rho_g\right) + \nabla.\left(\alpha_g\rho_g\,\vec{u}_g\right)\right] = 0 \tag{7}$$

$$\sum_{q=1}^{n}\alpha_q = 1 \tag{8}$$

Since the flow of air-water interfaces is tracked based on the distribution of the secondary phase (air) volume in a specified space and is considered the volume fraction of air α_g, which is

value varies from 0 for liquid phase (water) and 1 for gas phase (air), therefore the Eqs. (8) is reduced to:

$$\alpha_g + \alpha_L = 1 \quad (9)$$

and the bulk properties for the mixture depended on the volume fraction weighting and properties of each phase and found as:

$$\rho = \rho_L \alpha_L + \rho_g \alpha_g \quad (10)$$

$$\mu = \mu_L \alpha_L + \mu_g \alpha_g \quad (11)$$

The source term T_i is referred to the surface tension effect which is modeled using the continuum surface force (CSF) approach proposed by, **Brackbill et al., 1992,** as follows, **Fluent, 2012,** and**, Li et, al., 2012**:

$$\vec{T} = \sigma \frac{2\,\rho\, k \nabla \alpha_g}{(\rho_L + \rho_g)} \quad (12)$$

Where σ is surface tension coefficient, k is the local surface curvature and equals to:

$$k = \frac{\partial \dot{n}_i}{\partial x_i} \quad (13)$$

Where $\acute{n}$ is the unit normal.

3.2 Turbulence Model

In present study, a standard turbulence model (k- ε) is used for the system of the momentum equations, **Hanafizadeh et al., 2014.**

3.3 Geometry and coordinate systems

The proposed airlift pump is considered an external loop based on U- tube principle which is fed from reservoir with a constant head level of free surface and exposed to ambient pressure as shown in **Fig.4**. Because of the most major hydrodynamic changes happen when phases interface, therefore, the riser pipe is considered the main important part of the system to be under attention in mathematical modeling and is modeled as axisymmetric two- dimensional flow in cylindrical polar coordinates system, **Patankar, 1980.**

3.4 Boundary Conditions

1. Mass-Flow Inlet Boundary Condition

The inlet mass flow rate of injected air and turbulence conditions used in the present work are as follows:

Inlet mass flow rate is defined in vector terms as:

$$\vec{\dot{m}} = \dot{m} \cos\theta \; i + \dot{m} \sin\theta \; j \quad (14)$$

Where: $\dot{m} = 0.5, 2, 10, 50$ and 85 kg/hr

$\theta = 22.5$ and 90 dgree

Turbulence kinetic energy and dissipation rate are calculated as follow**, Versteeg and Malalasekera, 2007**:

$$k_{in} = \frac{3}{2}(u\, I)^2 \quad (15)$$

$$\varepsilon_{in} = C_\mu^{3/4} \frac{k^{3/2}}{l} \quad (16)$$

and

$$I = 0.16\ (Re)^{-1/8} \quad (17)$$

$$l = 0.07 D_h \quad (18)$$

Where: u = Inlet velocity.
I = Turbulence intensity.
C_μ = Universal constant, 0.09
l = Length scale of turbulence.
D_h = hydraulic diameter (pipe diameter).

2. Pressure Inlet Boundary Condition

A pressure inlet is specified for the free surface of water at the domain inlet where the pressure is atmospheric. An initial guess of turbulence kinetic energy and dissipation rate are calculated using Eqs. (15) and (16) and assuming turbulent intensity I is 0.05.

3. Pressure Outlet Boundary Condition

A pressure outlet boundary condition is assigned to the outlet of the domain where the pressure is atmospheric and no water back to the domain at the outlet (back flow volume fraction $\alpha = 1$). An initial guess of turbulence kinetic energy and dissipation rate are calculated using Eqs. (15) and (16) and assuming turbulent intensity I is 0.05.

4. Axisymmetry Boundary Condition

The axis symmetry of the domain is assigned to the center line of the riser pipe.

5. Wall Boundary Condition

No slip boundary condition is assigned for the internal wall of riser pipe. This condition is used to bound fluid and solid regions, **Jonas Bredberg, 2000**.

6. Interior Boundary Condition

The interior boundary conditions are appointed to the domain which is bounded by the solid wall of the riser pipe.

4. NUMERICAL SOLUTION

A control-volume technique is used for the solution, **Versteeg and Malalasekera, 2007,** and these methods are composed of the following stages:

- Generation of grid in the domain.
- Construction sets of algebraic of equations by integration of the governing equations on every control volume for the fields of velocity, pressure, void fraction and conserved scalars.
- Linearization and solving the discretized equations iteratively.

In the present work, the two phase flow is simulated as two-dimensional axisymmetry, unsteady, viscous and incompressible flow for both phases in an isolated airlift pump. Using GAMBIT 2.4.6, a two-dimensional uniform grid is generated for this purpose and contains non-overlapping rectangular element and an extra refinement is made at the air-water interface due to large variation in velocities and turbulence, as well as, near the solid wall, **Hitoshi et al., 2010**. A refined boundary layer mesh is created near the airlift pump wall to be able to resolve the velocity gradients better as shown in **Fig.5**. The spatial discretized is executed on a standard collocated grid applying finite volume method. The unsteady two-phase flow is modeled using VOF method and explicit scheme.

PISO algorithm of FLUENT 14.5 is used for the simulations. QUICK scheme for convective operator and a second order central difference scheme are used for the pressure term PRESTO scheme for pressure term and a second order. Upwind scheme is used for the momentum. Geo-Reconstruct scheme is used to represent the phases interface and predict the void fraction. The turbulent is modeled using $k-\varepsilon$ model. The inlet boundary conditions were the constant air mass flow rate, angle of injection, and constant pressure at the free surface. The outlet results of the program were the mixture mass flow rate and void fraction of each phase with distribution contours.

5. METHOD OF SOLUTION

The method of analysis includes the numerical solution of flow field equations:

1. Void fraction equation.
2. Continuity equation.
3. Momentum equation.
4. Transport equation of turbulence.

The solution algorithm implies modified version of PISO method of, **Issa, 1986,** which is considered an extension of SIMPLE method developed by, **Patanakar, 1980.** It is an iterative sequence consisting of two major parts: the PISO procedure, and the solution of transport equation. The PISO algorithm differs from SIMPLE algorithm by performing an extra correction step to the pressure and corresponding velocity field which are yielded from solving momentum equation using the correct pressure field or values predicted from the first correction step, after that the transport equations for turbulent and void fraction are solved using the new correct velocity field. The advantage for using PISO method in transient problem, that the accuracy reached by correction process (at each time step) for pressure is third order (Δt^3) and fourth order (Δt^4) for momentum. This yields an accuracy for the values of pressure and velocity filed (for a small time step) which is enough to travel to the next time step instantaneously without an extra iteration regarding the time as in SIMPLE method, therefore, PISO algorithm is considered as non-iterative method, **Versteeg and Malalasekera, 2007**. Changing the angles of air injection and mass rates of injected air, and the rate of pumped water is found in order to figure out the enhancement of the performance and efficiency of airlift pump.

6. AIRLIFT PUMP CHARACTERISTICS

The most important airlift pump characteristics in this work are the water pumping rate, and efficiency coefficients. Application of continuity and momentum conservation laws give amount of pumped water for specified operational and geometrical parameters. Once water flow rate is predicted, other pump characteristics can be found directly. Efficiency (η) of airlift pump is defined by, **Nicklin, 1963,** as a ratio of beneficial work done in water to the energy released from the isothermal expansion of injected air from injection pressure to the ambient pressure as following:

$$\eta = \frac{g\rho_L Q_L (L - H_s)}{P_a Q_g \ln(P_{in}/P_a)} \quad (35)$$

7. RESULTS

The mass flow rates of water that results from numerical simulation and experimental investigation of the tested airlift pump with injection angle ($90^{\circ} and\ 22.5^{\circ}$) at submergence ratio 0.75, are represented in **Fig.6**. It's clear from the figure that predicted mass flow rates for injection angle (22.5°) are higher than that the predicted for injection angle (90°) for the higher mass flow

rate of injected air with similar trend for both curves. This increase is related to the initial momentum of the injected air; in addition, the comparison between numerical results for water output from the pump and that predicted from the experimental work shows good agreement with average deviation about 11% and 9% for injection angle $90^{\circ} and\ 22.5^{\circ}$ respectively. The time history of water mass flow rate at the discharge side (exit) of the airlift pump which results from numerical solution are shown in **Figs.7, 8, 9, 10** and **11**. The average mass flow rate of discharged water for each mass flow rate of injected air is accounted after the system reach quasi-steady state and then taking the average value of water mass flow rate variation over the remained part of simulation time. In general, each one of these figures has unique behavior which is corresponding to a specify flow pattern, and this behavior can give a sense about the kind of flow pattern that occurs. **Fig.7** shows that there is no water that can be pumped for 0.5 kg/hr of injected air and this agrees with the experimental results because the mass flow rate of injected air is smaller than the minimum value of air mass flow rate required to initiate water discharge from the pump, which is about 1.8 kg/hr for both injection angle at the same submergence ratio 0.75. As the rate of air injection increased up 2 kg/hr, water starts to flow out from the pump and **Fig.8** shows the time history of water output at the exit of the pump. On inspection the figures it is noticed that the water induced to flow out from the pump after 3.75s (for angle 90°) and 3.5s (for angle 22.5°) then a slug of water arrives at the exit of the pump. After 3s approximately, the water slug is discharged and no flow region is dominated until the second slug of water arrives the exit approximately at time = 8s, and the sequence is repeated. It is clear that this sequence is corresponding to a specific flow pattern which is called slug flow. In the same manner, inspection of **Fig.9**, for air injection mass flow rate of 10kg/hr, shows similarity of behavior for both figures and the increasing of air injection mass flow rate cause increasing the unsteadiness of water flow at the pump exit, as well as, faster initiation of water discharge. Around time =1.8s, a large slug of water reaches at the exit of the pump and the second big slug reaches the exit at time= 7.7s, the flow between the two big slugs is decreasing then increasing and characterized with very unsteadiness flow, this description is reveals to slug-churn flow. Further increasing of mass flow rate of injected air up to 50kg/hr, the behavior of water flow rate with time loss its fashion and become more unsteady and chaotic as shown in **Fig.10.** More careful inspection of the behavior shows after water slug discharged at the exit of the pump, sharp decreasing followed by rapid gradual increasing of water mass flow rate until the next water slug arrives to the exit, this behavior is continuously repeated and this described the oscillatory motion of water slug which is revealed to churn flow. **Fig.11** shows the annular flow pattern that occurs with air mass flow rate of 85kg/hr, it is noticed that the local spikes are disappeared. This means there is no more slug of water and the flow at the exit is highly unsteady. The average water mass flow rate for each one of the theoretical **Figs.7, 8, 9, 10** and **11** are compared with flow map of, **Tailet et al., 1980,** as shown in **Fig.12**, and the distribution of the results on the map agrees fairly to that discussed above. Contours of air void fraction that results from the simulation of airlift pump are shown in **Fig.13** which is corresponding to bubble, slug, churn and annular flow. **Figs.14, 15** and **16** show the flow development with time in the riser pipe started from time = 0 second for mass flow rate of injected air (0.5, 2, and 50 kg/hr) respectively. It is observed, that there is no significant difference can be noticed in flow structure when the injection angle is changed from $90^{\circ} to\ 22.5^{\circ}$ for the same mass flow rate of injected air at same submergence ratio. Variation of the efficiency that is predicted numerically and experimentally with mass flow rate of injected air is present in **Fig.17**, which show agreement with average deviation about 6% and 5% for injection angle $90^{\circ} and\ 22.5^{\circ}$ respectively. The behavior of predicted numerical results for

efficiency and performance curve is compared to gather as shown in **Fig.18**. It is clear from the comparison that the maximum efficiency point does not occur with the maximum mass flow rate of water due to the transition of flow pattern from stable slug flow to churn flow which is characterized as chaotic and unstable add to that, the best efficiency points achieved when the flow is slug and slug-churn flow.

8. CONCLUSIONS

- The optimum angle of air injection was found to be at 22.5° for the selected operational and geometrical parameters.
- Average enhancement of airlift pump performance is about 11% for air injection angle 22.5°.
- There is no significant variation in flow structure when the air injection angle was changed from $90^{\circ}$to 22.5°.
- Water starts to flow out from the airlift pump when slug flow occurs, when the mass flow rate of injected air is 1.8 kg/hr.
- Maximum efficiency achieved is increased about 11% for air injection angle 22.5°.
- Maximum efficiency of airlift pump does not occur with the maximum mass flow rate of water.
- Best efficiency points corresponds to the slug and slug-churn flow pattern, therefore, it's recommended to operate any airlift pump with these patterns of flow.
- Numerical simulation using VOF model gave a fairly accurate result when compared with experimental.
- Numerical simulation using VOF model is capable to providing information about the flow patterns and transient nature of the flow.

NOMENCLATURE

A =cross section area of the riser pipe, m^2
c =color function
D_h=hydraulic diameter, m
g =gravity acceleration, m/s^2
H_s =static head or submerged length, m
I =turbulence intensity
k =turbulent kinetic energy, m^2/s^2
l =length scale of turbulence, m
L=length of riser pipe, m
$\dot{m}$=mass flow rate, kg/s
N=displacement in the wall normal direction or outward face area vector unit
$\hat{n}$=normal unit vector
P=pressure, N/m^2
Q =volume flow rate, m^3/s
Re=Reynolds number
T =surface tension, N
t=time, s
u =velocity, m/s
$\bar{u}$ =velocity vector, m/s
u_j=velocity in tenser notation, m/s
V =volume, m^3
x_i =position vector in tenser notation, m

α =volume fraction
δ_{ij}=kronecker symbol
θ =angle of air injection, dgree
κ =Von Karman's constant in the velocity log-law
ε =dissipation of turbulent kinetic energy, m^2/s^3
μ =molecular or dynamic viscosity, kg/m.s
μ_t=turbulent eddy viscosity, kg/m.s
ρ =density, kg/m^3
σ =surface tension coefficient, N/m
τ =shear stress, N/m^2
τ_{ij}=viscous stress tensor, N/m^2
η =efficiency

REFRENCES

- Aaron Bohnen D., 2004, *Air-actuated technology in urban drainage*, M.Sc. thesis, Civil Eng. Dep., The University of British Columbia.
- Brackbill J. U., D. B. Kothe, C. Zemach, 1992, *A Continuum method for modeling surface tension*, Journals of computational physics, Vol. 100, pp. 335-354.
- Ferziger, J.H., Peric, M., 2002, *Computational Methods for Fluid Dynamics*, 3rd rev. Edition Springer, Berlin.
- Fluent Program, 2012, *Fluent 14.5 User's Guide, programming and Tutorial Guide* Fluent, Version 14.5, Ansys Inc.
- Hanafizadeh Pedram, Mahsa Moezzi, Mohammad Hassan Saidi, 2014, *Simulation of gas-liquid two phase flow in upriser pipe of gas-lift systems*, Energy Equipment and Systems, Vol 2, pp. 25-41.
- Hirt C. W., B. D. Nichols, 1981, *Volume of fluid (VOF) Method for the dynamics of free boundaries*, Journals of computational physics, Vol.39, pp. 201-225.
- Hitoshi F., M. Kubo, T. Hama, H. Takuda, 2010, *Transport phenomena of solid particles in pulsatile flow*, Kyoto University, Advance in Mechanical engineering, Vol. 2010, pp. 1-15.
- Issa Raad I., 1986, *Solution of the implicitly discretized fluid flow equations by operator splitting*, Journals of Computational Physics, Vol. 62, pp. 40-65.
- Jonas Bredberg, 2000, *On the wall boundary condition for turbulence models*, Department of thermo and fluid dynamics, Chalmers university of technology, Sweden. Internal report, 00/4.
- Kassab Sadek Z., Hamdy A. Kandil, Hassan A. Warda, Wael H. Ahmed, 2009, *Air-lift pumps characteristics under two-phase flow conditions*, International Journal of Heat and Fluid Flow, Vol.30, pp. 88–98.
- Li X. S., H. M. Jeong and H. S. Chung, 2012, *CFD Modeling of Unsteady Gas-Liquid Flow in a Small Scale Air-Lift Pump,* Korean power system engineering, pp.30-37.
- Mahrous, 2014, *Performance of Airlift Pumps: Single-Stage vs. Multistage Air Injection*, American Journal of Mechanical Engineering, Vol. 2, pp. 28-33.
- Nicklin D. J., 1963, *The airlift pump theory and optimization*, International chemical Eng., Vol. 41, pp. 29-39.
- Patankar V. Suhas, 1980, *Numerical Heat Transfer and Fluid Flow*, Series in Computational Methods in Mechanics and Thermal Sciences. Hemisphere Publ. Corp., McGraw-Hill.

- Qingsong Zhang, Li Xu , 2015, *A simulation of air-lift artificial upwelling in vertical pipe*, International Conference on Intelligent Systems Research and Mechatronics Engineering.
- Reinemann D. J., J. Y. Parlange, M. B. Timmons, 1990, *Theory of Small-Diameter Airlift Pump*, I. J. Multiphase flow, Vol. 16, pp. 113-122.
- Sakr I. M., W. A. El-Askary, A. Balabel, K. Ibrahim, 2012, *Computational of Upward Water/Air Fluid Flow in Vertical Pipe*, CFD Letters, Vol.4, pp.193-213.
- Stenning, A.H., Martin, C.B., 1968, *An analytical and experimental study of air lift pump performance*, J. Eng. Power, Trans. ASME' Vol. 90, pp.106–110.
- Taitel Yehuda, Dvora Bornea, A. E. Dukler, 1980, *Modeling Flow Pattern Transitions for Steady Upward Gas-Liquid Flow in Vertical tubes*, AICh journal, Vol. 26, No. 3, pp. 345-354.
- Versteeg, H. K., Malalasekera W., 2007, *An introduction to computational fluid dynamics-The finite volume method*, Longman group Ltd. 2nd edition.
- Wahba E. M., M. A. Gadalla, D. Abueidda, A. Dalaq, H. Hafiz, K. Elawadi and R. Issa, 2014, *On the Performance of Air-Lift Pumps: From Analytical Models to Large Eddy Simulation*, Journal of FluidsEngineering, Vol. 136, pp.1-7.
- White F. W., 1991, *Viscous Fluid Flow*, 2nd Edition, University of Rhode Island, McGraw-Hill, Inc. New York.

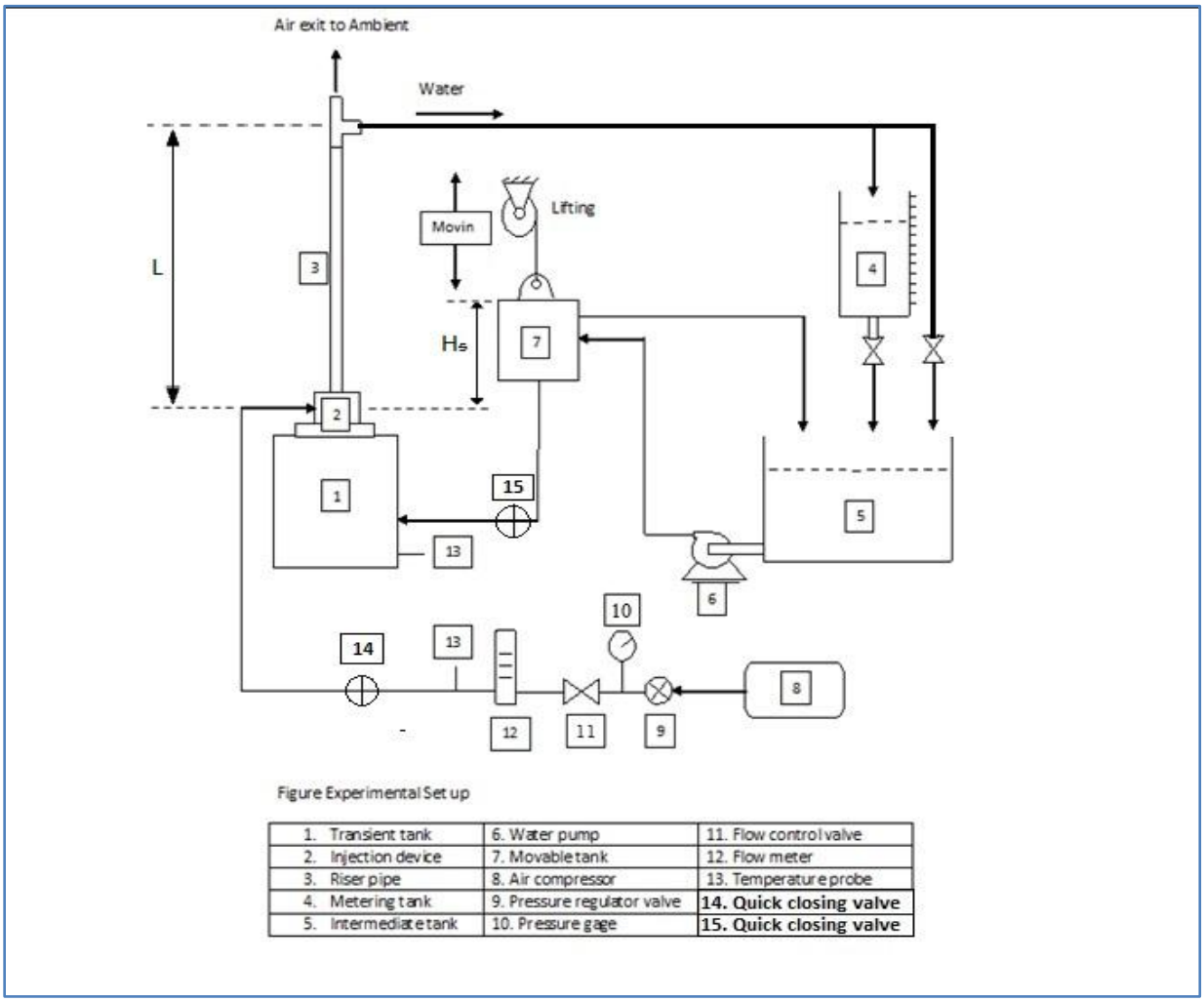

Figure Experimental Set up

1. Transient tank	6. Water pump	11. Flow control valve
2. Injection device	7. Movable tank	12. Flow meter
3. Riser pipe	8. Air compressor	13. Temperature probe
4. Metering tank	9. Pressure regulator valve	**14. Quick closing valve**
5. Intermediate tank	10. Pressure gage	**15. Quick closing valve**

Figure 1. Testing schematics.

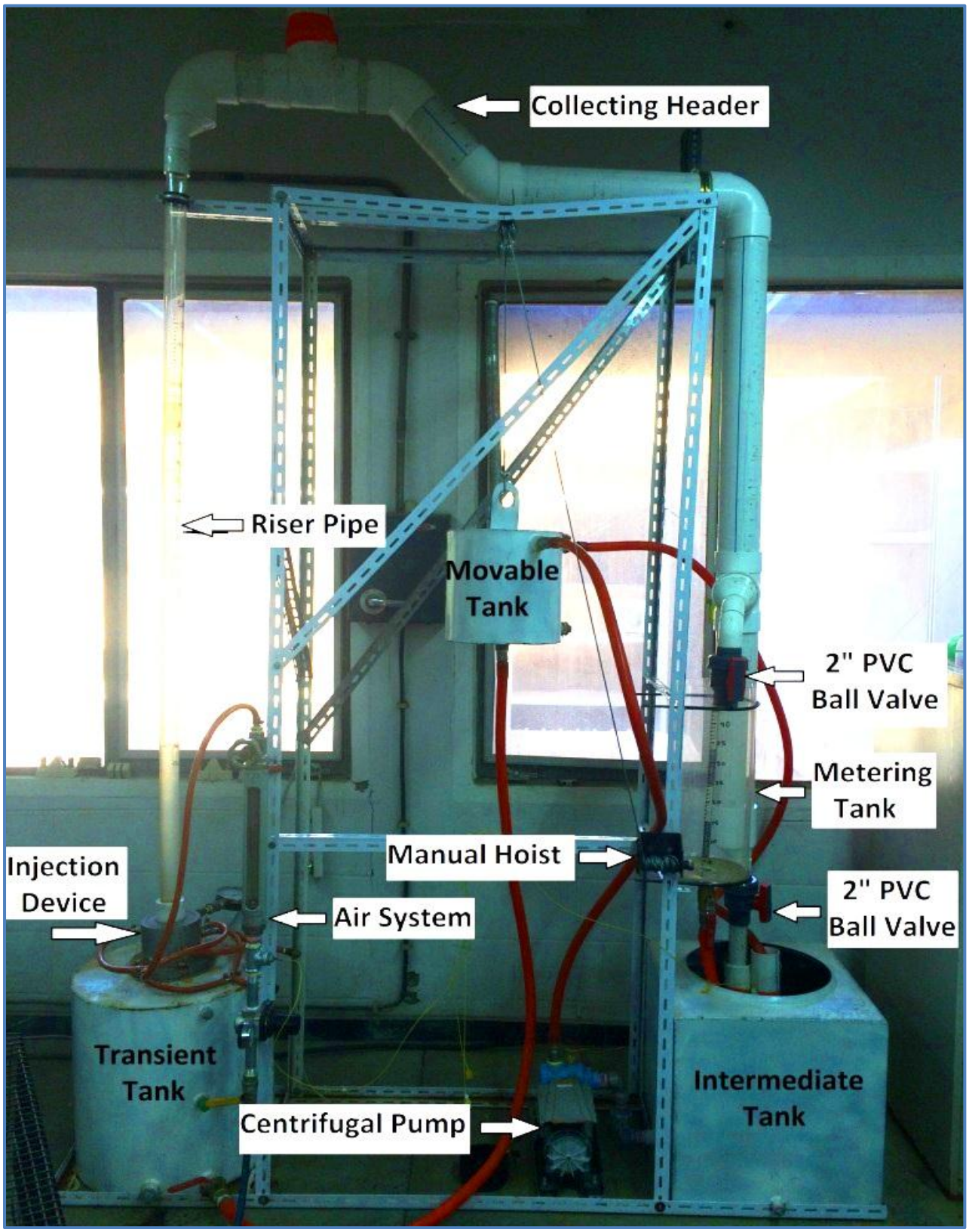

Figure 2. Experimental setup.

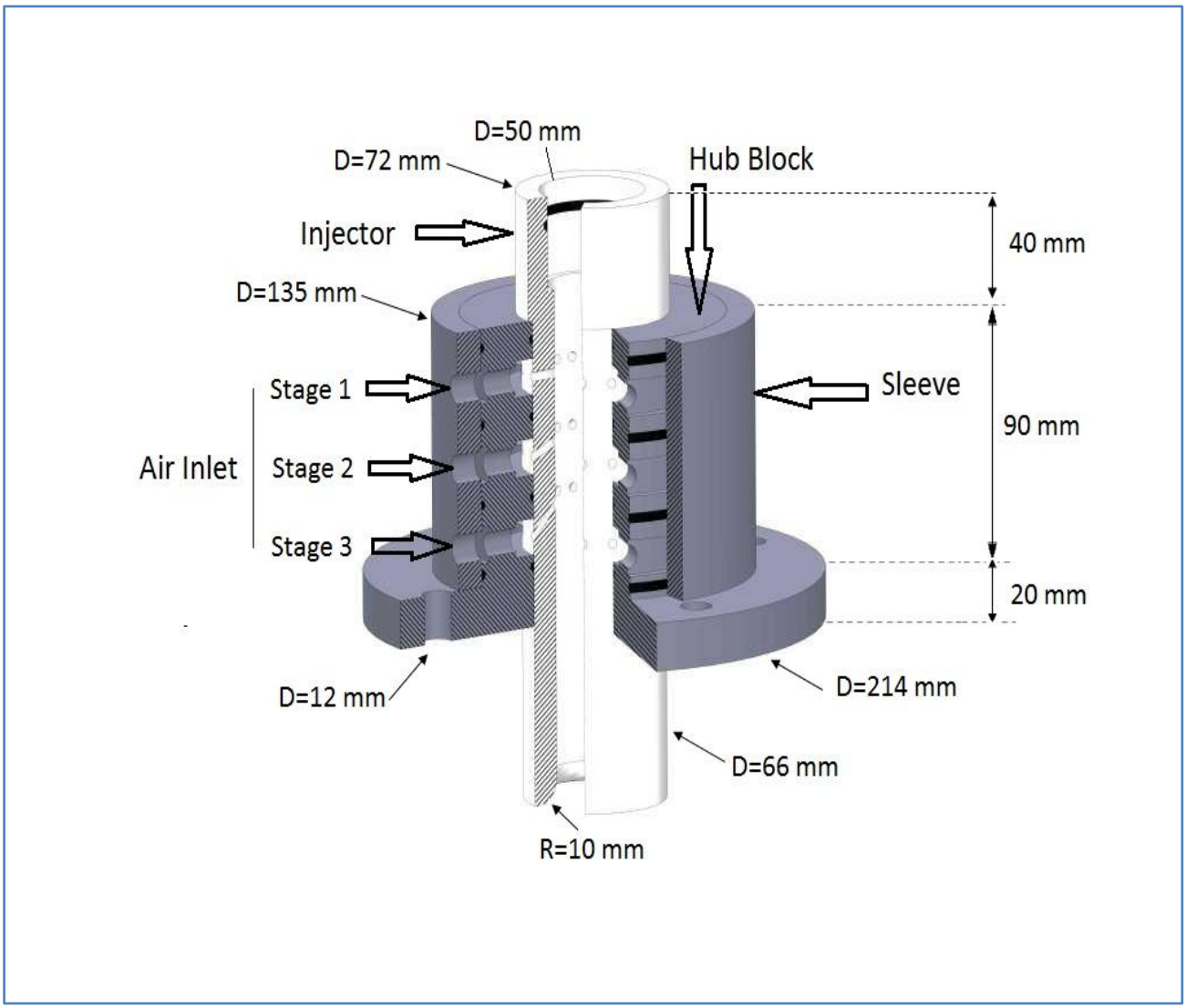

Figure 3. Cross section of injection device.

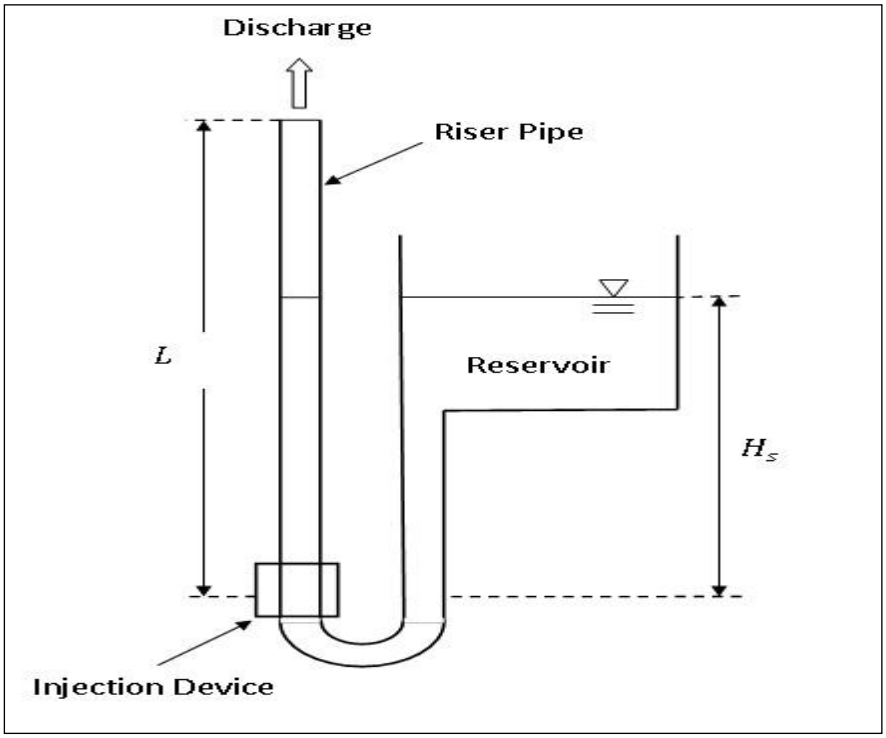

Figure 4. Proposed airlift pump as U-tube concept.

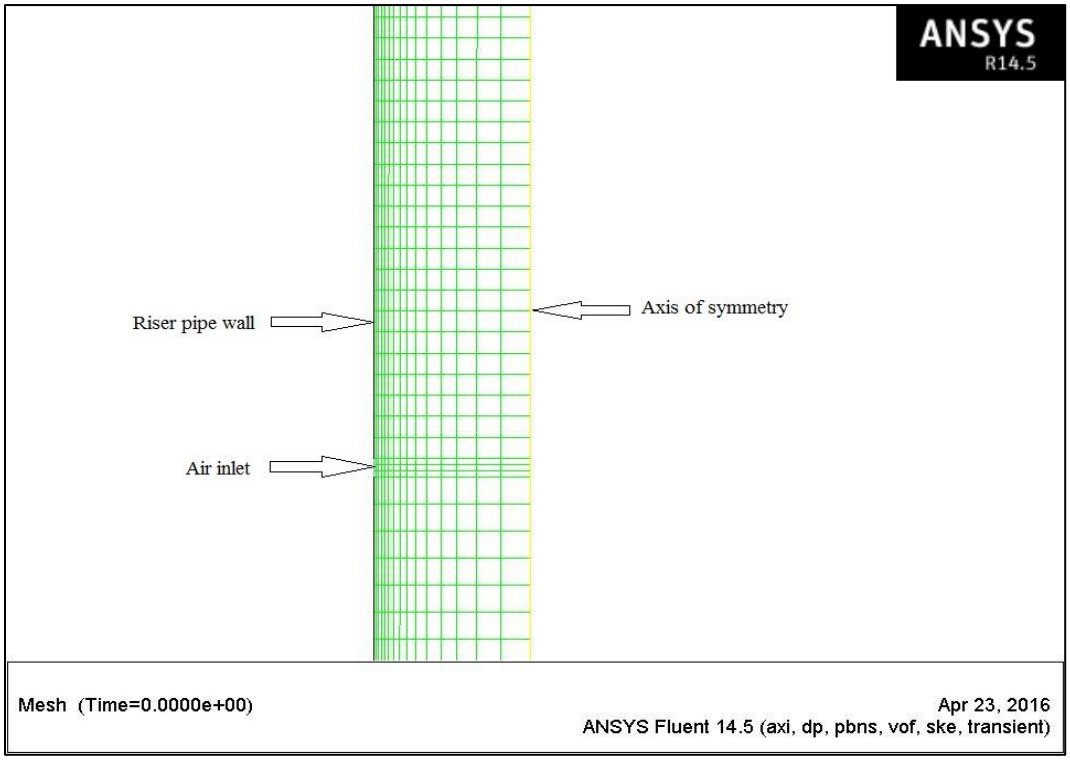

Figure 5. Two-dimensional axisymmetry representation.

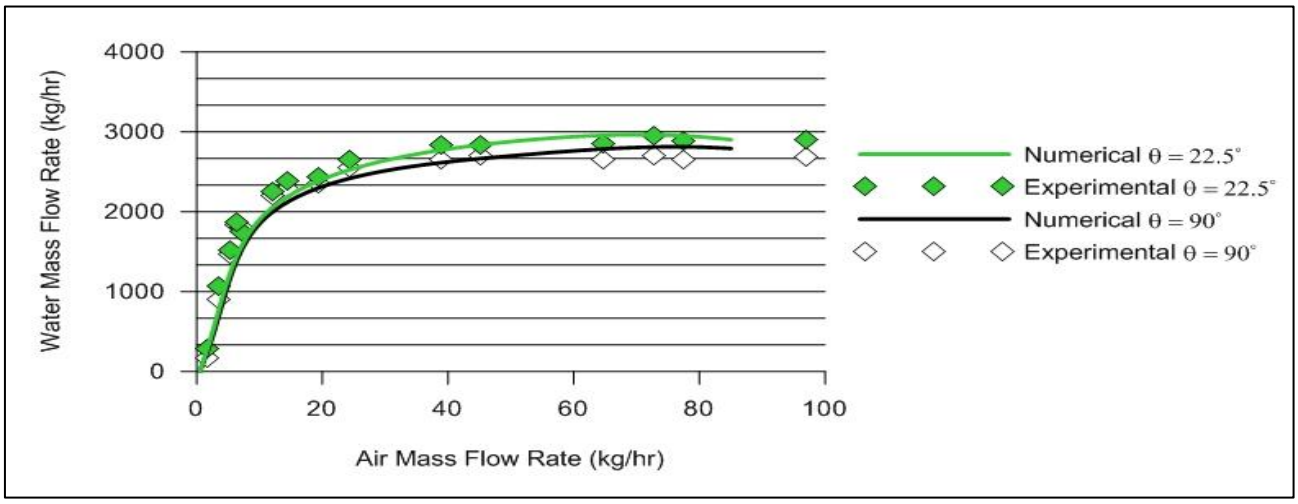

Figure 6. Variation of airlift pump performance curve with injection angles.

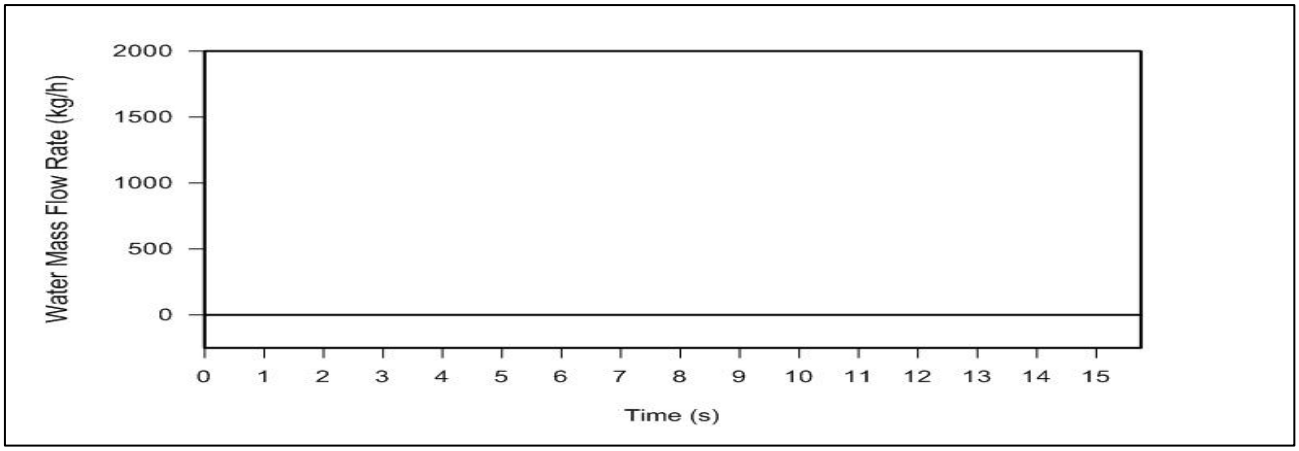

Figure 7. Numerical results for water mass flow rate predicted at the discharge of the riser pipe at air mass flow rate (0.5 kg/hr), and injection angle 90°.

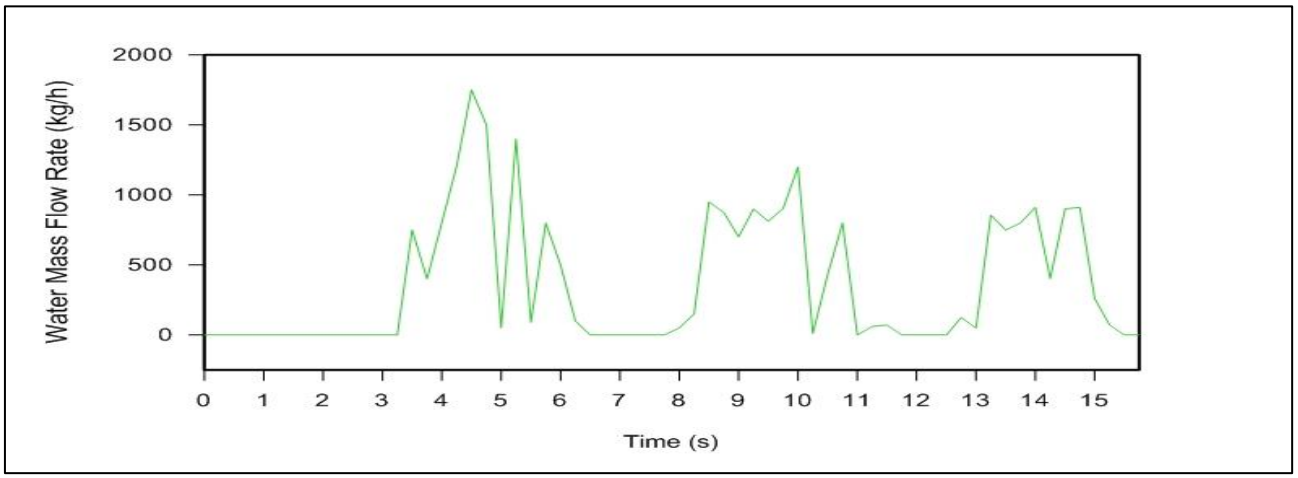

Figure 8. Numerical results for water mass flow rate predicted at the discharge of the riser pipe at air mass flow rate (2 kg/hr), and injection angle 22.5°.

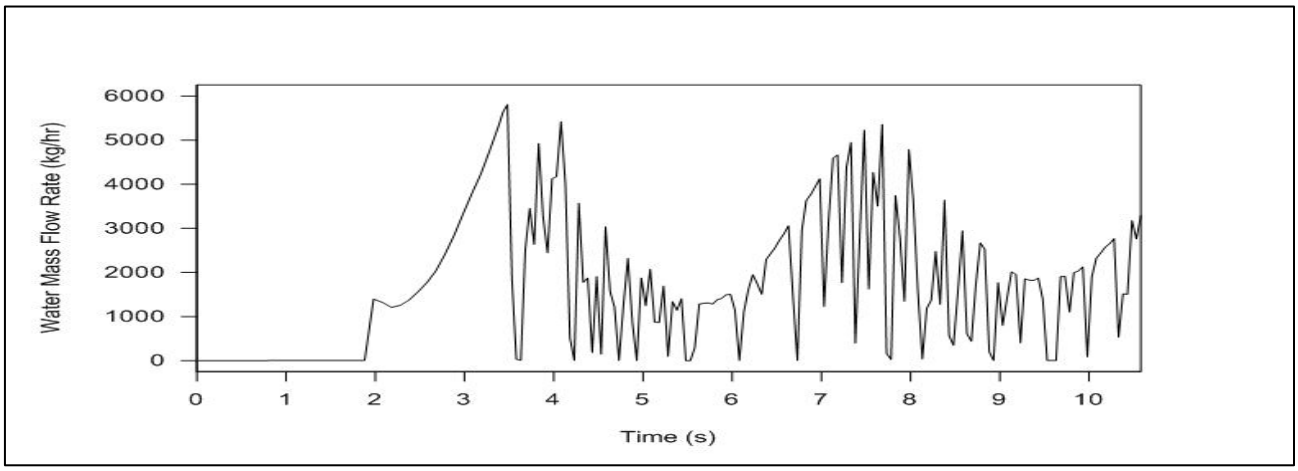

Figure 9. Numerical results for water mass flow rate predicted at the discharge of the riser pipe at air mass flow rate (10 kg/hr), and injection angle 90°.

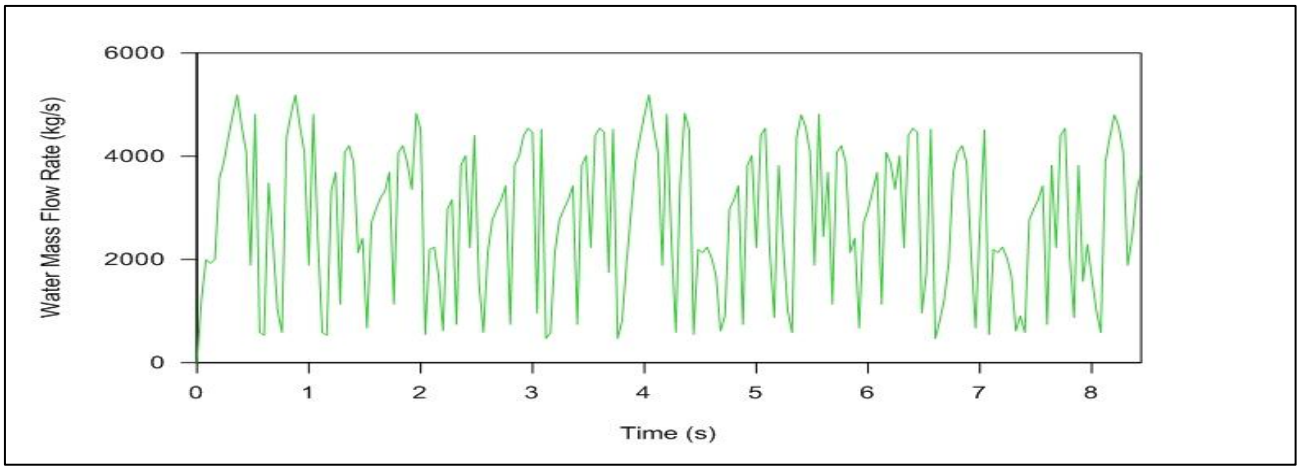

Figure 10. Numerical results for water mass flow rate predicted at the discharge of the riser pipe at air mass flow rate (50 kg/hr), and injection angle 22.5°.

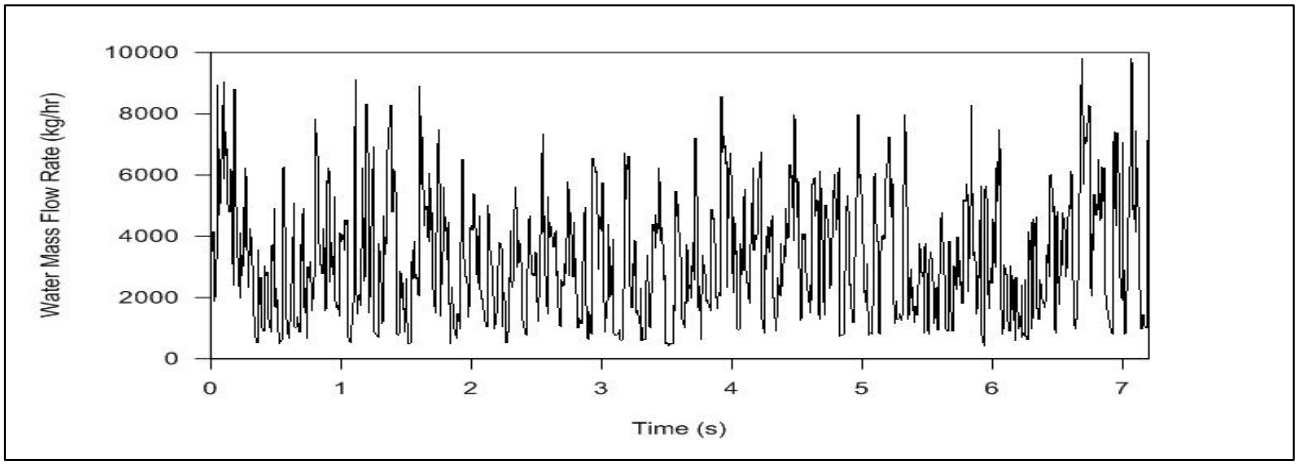

Figure 11. Numerical results for water mass flow rate predicted at the discharge of the riser pipe at air mass flow rate (85 kg/hr), and injection angle 90°.

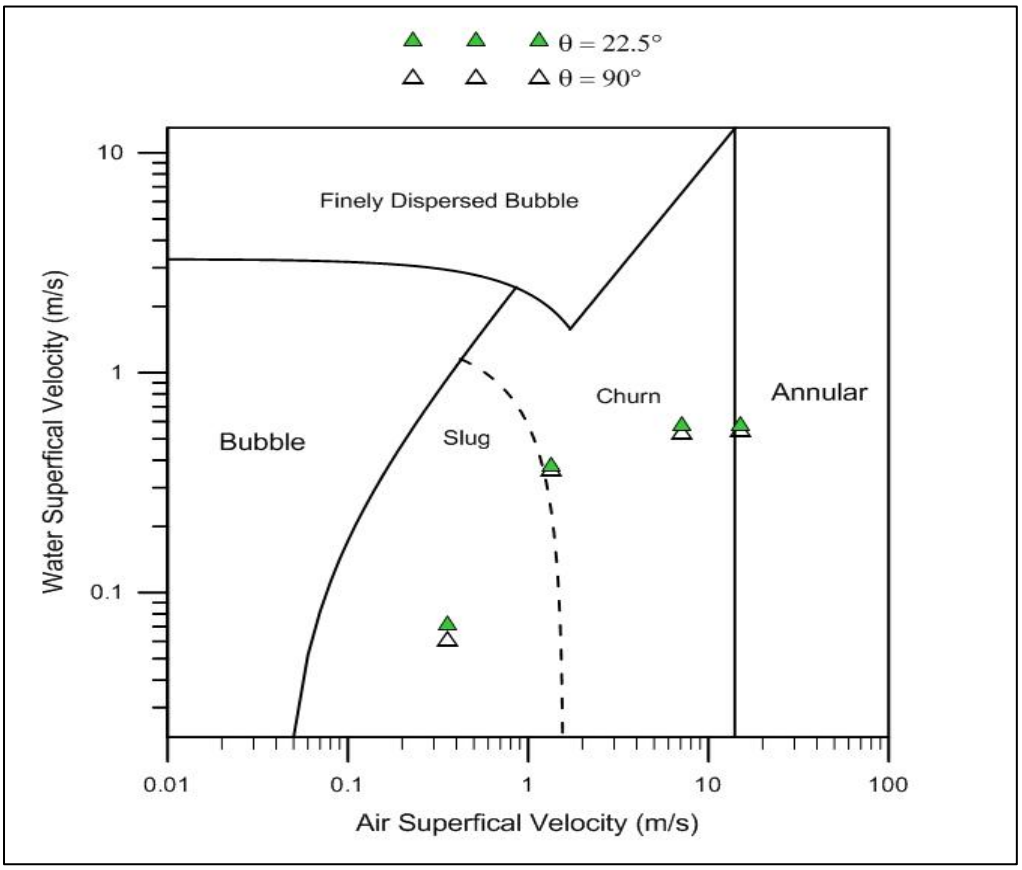

Figure 12. Distribution of numerical and experimental results for various injection angles on the flow map proposed by, **Taitel et al., 1980**.

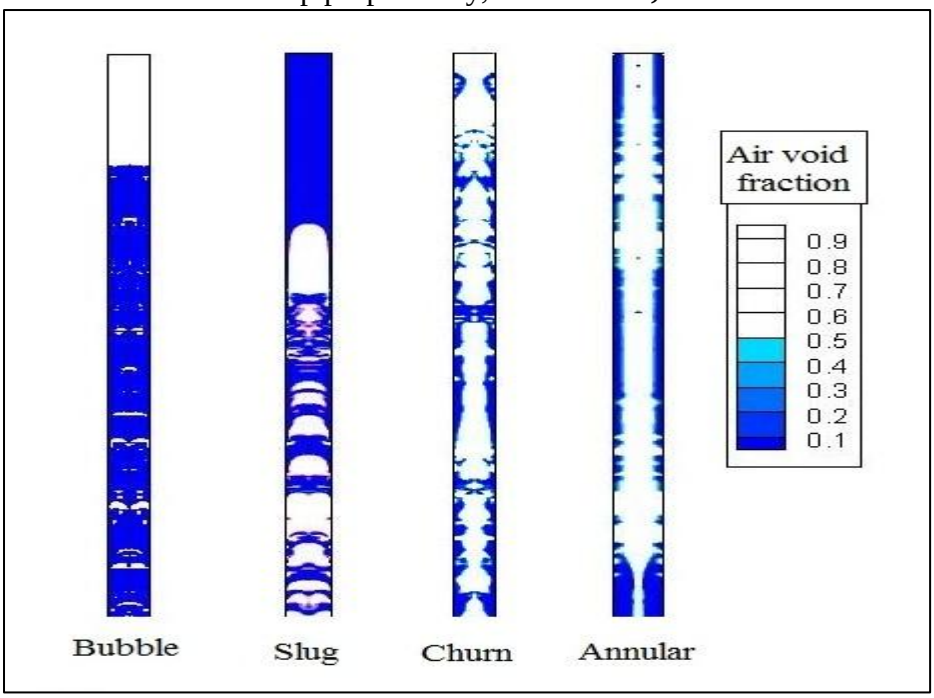

Figure 13. Obtained flow patterns from simulation.

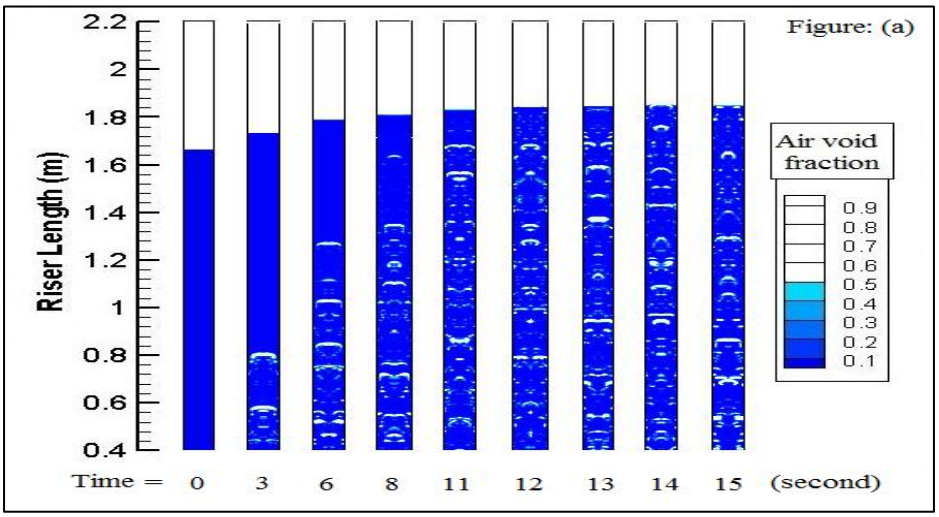

Figure 14. Variation of air void fraction contours at air mass flow rate (0.5 kg/hr) and angle 90°.

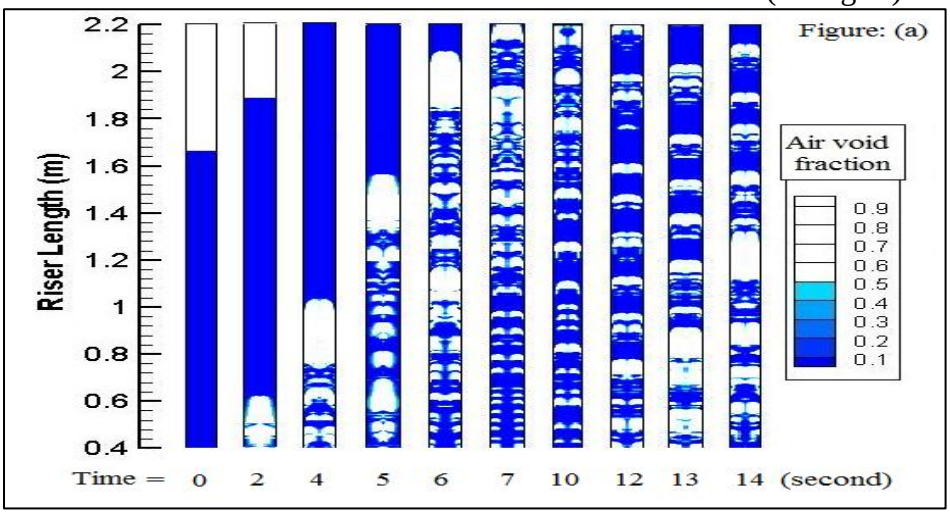

Figure 15. Variation of air void fraction contours at air mass flow rate (2 kg/hr) and angle 22.5°.

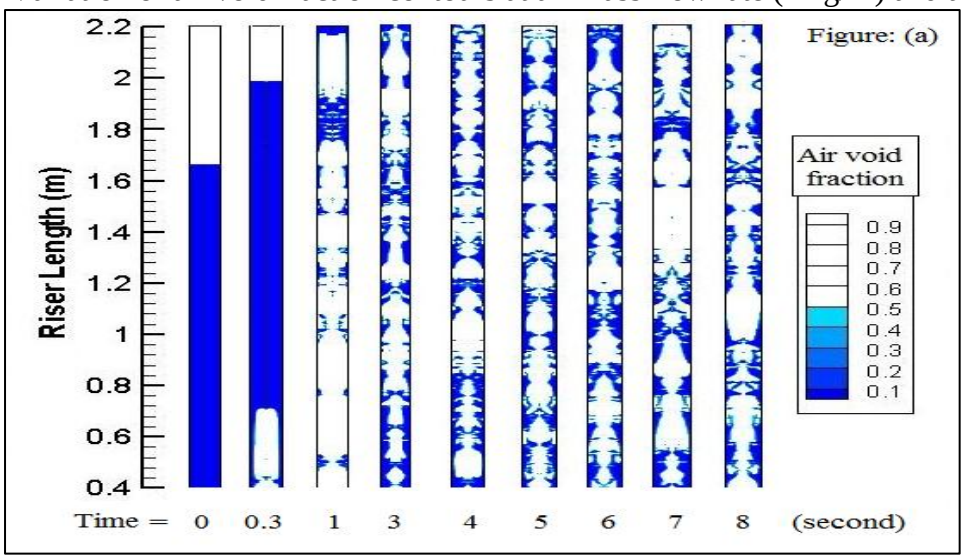

Figure 16. Variation of air void fraction contours at air mass flow rate (50 kg/hr) and angle 22.5°.

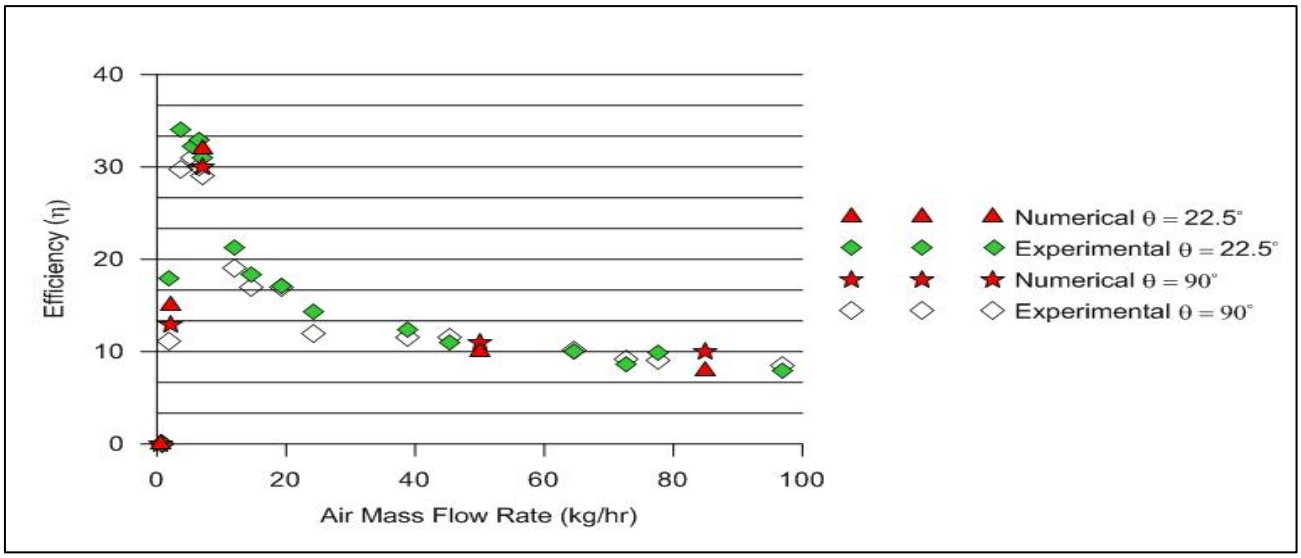

Figure 17. Variation of airlift pump efficiency with injection angle.

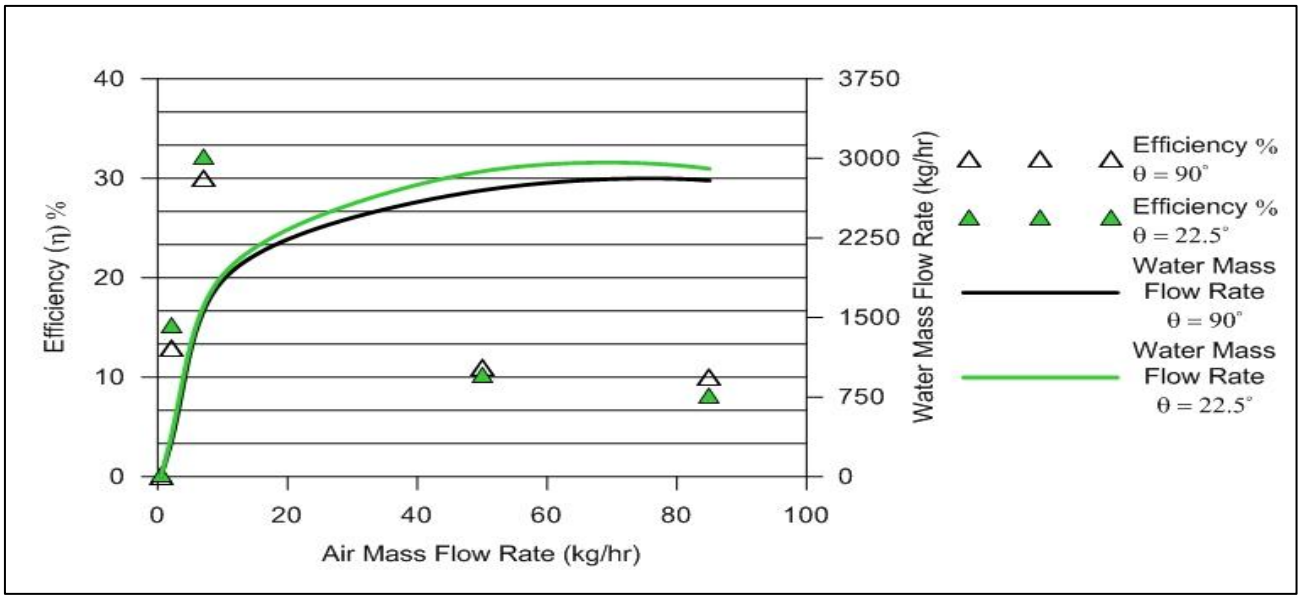

Figure 18. Variation of numerical predicted efficiency of airlift pump with performance curve.